

# How to Train Your Dragon: Tamed Warping Network for Semantic Video Segmentation

Junyi Feng<sup>1</sup> · Songyuan Li<sup>1</sup> · Xi Li<sup>1</sup>

Received: date / Accepted: date

**Abstract** Real-time semantic segmentation on high-resolution videos is challenging due to the strict requirements of speed. Recent approaches have utilized the inter-frame continuity to reduce redundant computation by warping the feature maps across adjacent frames, greatly speeding up the inference phase. However, their accuracy drops significantly owing to the imprecise motion estimation and error accumulation. In this paper, we propose a framework named Tamed Warping Network (TWNNet) to introduce a simple and effective correction stage right after the warping stage, aiming to improve the accuracy and robustness of warping-based models. The experimental results on the Cityscapes dataset show that with the correction, the accuracy (mIoU) significantly increases from 67.3% to 71.6%, and the speed edges down from 65.5 FPS to 61.8 FPS. For non-rigid categories such as “human” and “object”, the improvements of IoU are even higher than 18 percentage points.

**Keywords** Semantic Video Segmentation, Feature Correction, Warping, Real-Time

Junyi Feng and Songyuan Li have contributed equally to this work.

✉ Xi Li  
xilizju@zju.edu.cn

Junyi Feng  
fengjy@zju.edu.cn

Songyuan Li  
leizungjyun@zju.edu.cn

<sup>1</sup> College of Computer Science and Technology, Zhejiang University, 38 Zheda Road, Hangzhou, 310027, China

## 1 Introduction

Semantic video segmentation aims at generating a sequence of pixel-wise class label maps for each frame in a video. A real-time solution to this task is challenging due to the stringent requirements of speed and space. Prevailing real-time methods can be grouped into two major categories: per-frame methods and warping-based methods. Per-frame methods decompose the *video* task into a stream of mutually independent *image* segmentation tasks. They usually reduce the resolution of input images (Badrinarayanan et al., 2017; Li et al., 2019a; Yu et al., 2018) or adopt a lightweight CNN (Howard et al., 2017; Li et al., 2019a,b; Orsic et al., 2019; Sandler et al., 2018; Yu et al., 2018; Zhang et al., 2019b; Zhao et al., 2018) to meet the real-time demand. In light of the visual continuity between adjacent video frames, warping-based approaches (Gadde et al., 2017; Jain and Gonzalez, 2018; Li et al., 2018; Xu et al., 2018; Zhu et al., 2017) utilize some inter-frame motion estimation (e.g., optical flows (Xu et al., 2018; Zhu et al., 2017) or motion vectors (Jain and Gonzalez, 2018)) to avoid redundant computations, propagating (or *warping*) the segmentation results from the previous frame to the current one.

Although existing warping-based methods significantly boost the inference speed by saving the computational time for numerous redundant frames, their performance drops considerably due to the following limitations. 1) Every pixel in a non-key frame is estimated by motion flows from some pixels in the previous frame. Such estimation may work for continuous regions in a video, but the *moving of a non-rigid object* such as a human usually becomes **severely deformed**, as shown in Fig. 1(a), since a non-rigid object in a new frame can contain a considerable amount of new pixels which can-

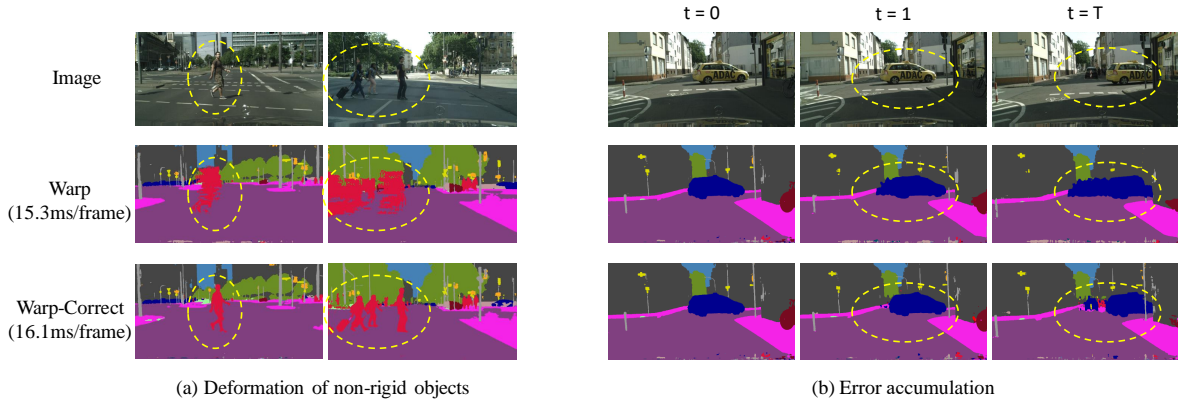


**Fig. 1** Qualitative results. The warped results are shown in the second row. (a) Non-rigid moving objects suffer **deformation**. (b) Warping results in **error accumulation** along consecutive non-key frames. By adding the lightweight correction stage, these two kinds of problems are significantly alleviated as shown in the third row.

not be estimated from the previous frame. 2) **Errors accumulate** along consecutive non-key frames, making the results of later frames almost unusable, as shown in Fig. 1(b). All in all, warping behaves like a runaway fierce creature. The key to the issue is to tame it — to take advantage of its acceleration and to keep it under control.

To deal with the issues above, we propose to introduce a lightweight correction stage after the warping stage, resulting in a novel framework, Tamed Warping Network (TWNNet), which contains a novel architecture and two correction modules for every non-key frame. First, we propose the non-key-frame CNN (NKFC) to perform segmentation for non-key frames. As shown in Fig. 2, NKFC fuses warped deep features from a previous frame with the features from its shallow layers, making itself fast and able to retain spatial details, the requisites to do the following correction. To alleviate the issue of deformation, we introduce a correction stage consisting of two modules. We design the context feature rectification (CFR) module to correct the warped features with the help of spatial details contained in NKFC. To help CFR focus on error-prone regions, we design the residual-guided attention (RGA) module to utilize the *Residual Maps* in the compressed domain. It is worth noting that TWNNet alleviates error accumulation in that it corrects every non-key frame rather than indulging the warping without restriction.

We evaluate TWNNet on the Cityscapes (Cordts et al., 2016) and CamVid (Brostow et al., 2009) datasets. Experimental results show that TWNNet greatly improve the accuracy and robustness of warping-based models. Specifically, for the  $1024 \times 2048$  videos on Cityscapes, the accuracy (mIoU) significantly increases from 67.3% to 71.6% by adding the correction, and the speed edges down from 65.5 FPS to 61.8 FPS. Furthermore, we

found the performance improvements of non-rigid categories such as “human” and “object” are even higher than 18 percentage points.

The main contributions of this work are summarized as follows:

- We propose a novel framework, Tamed Warping Network (TWNNet), to improve the performance of warping-based segmentation models by introducing a lightweight correction stage.
- We propose two efficient correction modules, the Context Feature Rectification module as well as the Residual-Guided Attention module, to alleviate the non-rigid object deformation and error accumulation problems during feature warping.
- Experimental results on Cityscapes and CamVid demonstrate that the proposed TWNNet framework greatly improves the robustness and accuracy.

## 2 Related Work

### 2.1 Feature Fusion in Semantic Segmentation

Semantic segmentation in an FCN manner (Long et al., 2015) has achieved remarkable accuracy. Recently, high-quality models (Chen et al., 2018; Huang et al., 2019; Zhang et al., 2019a; Zhao et al., 2017; Zhu et al., 2019; Fu et al., 2019; He et al., 2019) as well as high-speed lightweight approaches (Li et al., 2019a; Orsic et al., 2019; Yu et al., 2018; Zhao et al., 2018) show the importance of feature fusion from different layers (or scales). Generally, shallow layers contain more low-level *spatial* details, while deep layers more *contextual* information. The combination of features from different layers significantly improve the accuracy.

Feature fusion in our proposed non-key-frame CNN is similar to those in FPN (Lin et al., 2017) and U-

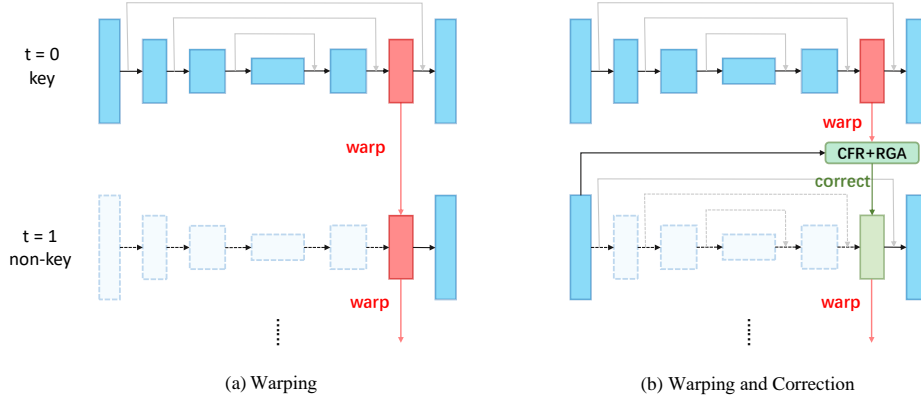


**Fig. 2** (a) Commonly-used warping-based approaches. (b) Our TWNet. Black arrows denote the main path of the network, while gray arrows denote the lateral connections (Lin et al., 2017). The warped layers are indicated by red color. The dotted arrows and boxes denote skipped operations.

Net (Ronneberger et al., 2015), where lateral connections are used to fuse the low-level (spatial) and high-level (context) features. In comparison, our non-key-frame CNN only retains a small number of layers of the encoder to extract low-level features and obtains high-level features by interior feature warping. Thus, the non-key-frame CNN saves the heavy computations of context feature extraction.

## 2.2 Warping-Based Video Segmentation

In general, videos are of temporal continuity, i.e., consecutive video frames look similar, making it possible to perform inter-frame prediction. The process of mapping pixels from the previous frame to the current one according to a pixel-level motion map is called image warping (Fig. 3). Each point in the motion map is a two-dimensional vector,  $(\Delta x, \Delta y)$ , representing the movement from the previous frame to the current one. Motion vectors and optical flows are two kinds of commonly used motion maps. In general, motion vectors, already contained in videos, are less precise than optical flows (e.g., TV-L1 (Zach et al., 2007) FlowNet2.0 (Ilg et al., 2017) and PWC-Net (Sun et al., 2018)). However, it takes extra time to perform optical flow estimation.

Researchers have proposed many warping-based semantic video segmentation approaches (Gadde et al., 2017; Jain and Gonzalez, 2018; Xu et al., 2018; Zhu et al., 2017). Gadde et al. (Gadde et al., 2017) proposed to enhance the features of the current frame by adding it with the warped features from previous frames. Zhu et al. (Zhu et al., 2017), Xu et al. (Xu et al., 2018) and Jain et al. (Jain and Gonzalez, 2018) proposed to use feature warping for acceleration. They divided frames into two types, key frames and non-key frames. Key

frames are sent to the CNN for segmentation, while non-key frame results are obtained by warping. Recently, Hu et al. (Hu et al., 2020) proposed to approximate high-level features by composing features from several shallower layers. These warping-based approaches efficiently speed up the inference phase since the computational cost of warping is much less than that of CNN. However, both the accuracy and robustness of these methods deteriorate due to the following reasons. First, neither optical flows nor motion vectors can estimate the precise motion of all pixels. Thus, there always exist unavoidable biases (errors) between the warped features and our expected ones. Second, in the case of consecutive non-key frames, the errors accumulate fast, leading to unusable results. To address the error accumulation problem, Li et al. (Li et al., 2018) and Xu et al. (Xu et al., 2018) proposed to adaptively select key frames by predicting the confidence score for each frame. Jain et al. (Jain and Gonzalez, 2018) introduced bi-directional features warping to improve accuracy. However, all these approaches lack the ability to correct warped features.

## 3 Preliminaries: Warping and Correction in Video Codecs

In this section, we describe the basics and the pipeline of warping-correction in video codecs. Warping is an efficient operation for inter-frame prediction. Given the previous frame  $I_{t-1}$  and the motion vectors of the current frame  $Mv_t$ , we can estimate the current frame  $\hat{I}_t$  by image warping. The process is described as

$$\hat{I}_t = \text{warp}(I_{t-1}, Mv_t). \quad (1)$$

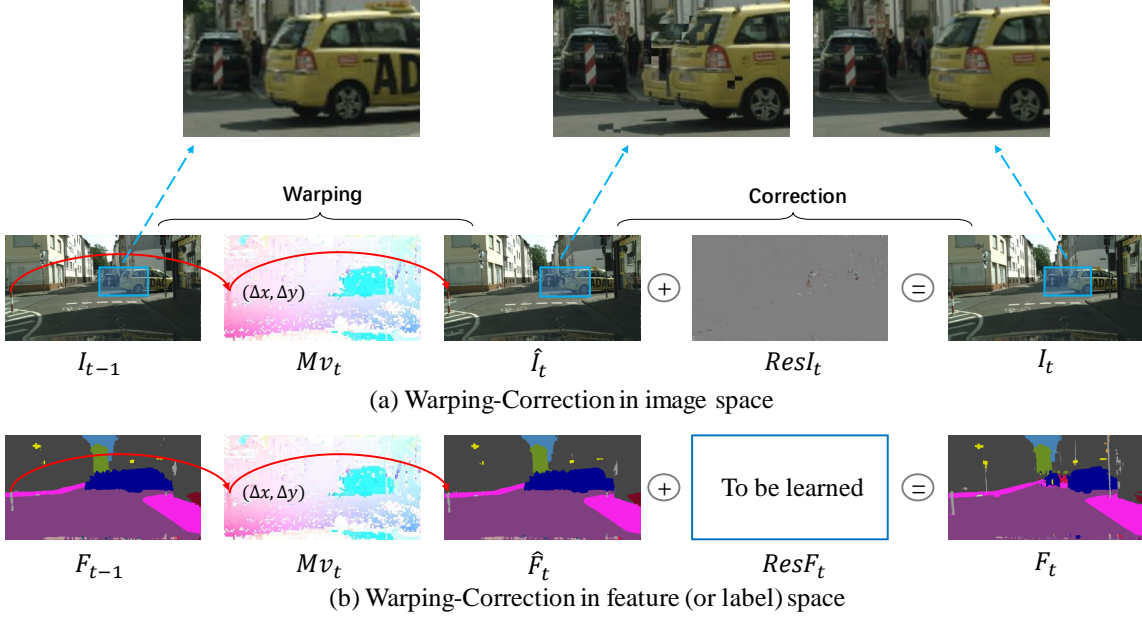


**Fig. 3** Visualization of **Warping** and **Correction**. (a) In image space, video codecs first warp the previous frame to the current one, then add the image-space residual map for correction. (b) We propose to learn the **residual in feature space** to rectify the warped features. Note that for better visualization, we use segmentation labels to represent features.

For a particular location index  $p \in \mathcal{Z}^{H \times W}$  in an image, the mapping function is given by

$$\hat{I}_t[p] = I_{t-1}[p - Mv_t[p]]. \quad (2)$$

However, there always exist biases between the warped image and the real one, especially in some complicated scenes and for the non-rigid moving objects. In order to correct the biases in image space, modern video codecs (e.g., MPEG (Le Gall, 1991), H.264 (Sofokleous, 2005)) add a correction step after image warping (Fig.3(a)). Specifically, the codec performs pixel-wise addition between the warped image  $\hat{I}_t$  and the *residual map*  $ResI_t$  to make correction. Each point in  $ResI_t$  is a three-dimensional vector,  $(\Delta r, \Delta g, \Delta b)$ , which describes the color differences between the warped pixel and the expected one. The overall inter-frame prediction process is described as

$$I_t = \text{warp}(I_{t-1}, Mv_t) + ResI_t. \quad (3)$$

The correction step effectively addresses the bias problem and the error accumulation problem in image space. Inspired by this, **we propose to learn the residual term in feature space** (Fig. 3(b)) to alleviate problems incurred by feature warping.

## 4 Tamed Warping Network

In this section, we introduce the Tamed Warping Network (TWNNet). We first outline the overall framework.

Next, we introduce our non-key-frame CNN architecture and the correction modules, i.e., the Context Feature Rectification (CFR) module as well as the Residual-Guided Attention (RGA) module. Finally, we present the implementation details.

### 4.1 Overview

The whole framework of Tamed Warping Network (TWNNet) is illustrated in Fig. 4. In our framework, video frames are divided into key frames (I-frames) and non-key frames (P-frames). The key frames are sent to the key-frame CNN (an U-shape (Lin et al., 2017; Ronneberger et al., 2015) FCN) where the context features of a selected interior layer are sent (warped) to the next frame. For non-key frames, the warped features are first corrected by the Context Feature Rectification (CFR) and Residual-Guided Attention (RGA) modules and then fused with the spatial features of the current frame. Then, the resultant features are used to make prediction and also sent to the next frame. The components of TWNNet are described as follows.

### 4.2 Basic Model: The Non-Key-Frame CNN

Warping can be applied in feature space (Fig. 3(b)) since the “conv” layers in FCN models preserve the position information. Given the features of the previous

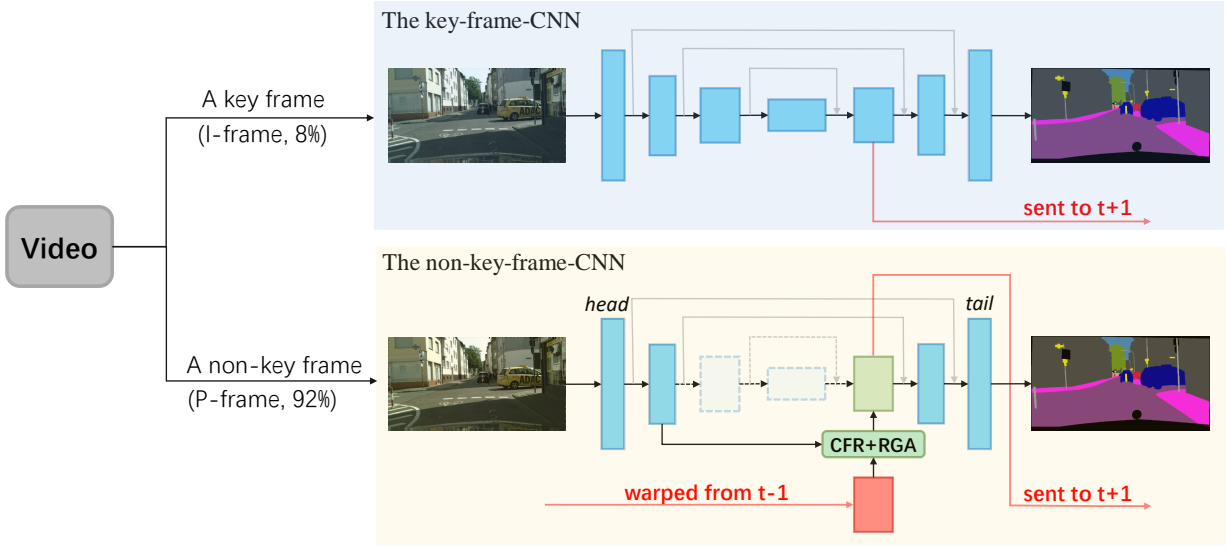


**Fig. 4** The framework of Tamed Warping Network. The key-frames (I-frames) are sent to the key-frame CNN. The non-key frames (P-frames) are sent to the non-key-frame CNN, where the warped context features are first corrected by the CFR and RGA modules and then fused with the spatial features extracted from the current frame. Both branches output the result label maps and the interior context feature maps.

frame  $\mathcal{F}_{t-1}$ , we can use  $Mv_t$  to predict the features of the current frame  $\hat{\mathcal{F}}_t$  by

$$\hat{\mathcal{F}}_t = \text{warp}(\mathcal{F}_{t-1}, Mv_t). \quad (4)$$

In this work, we propose the non-key-frame CNN architecture as the basic model to perform segmentation for non-key frames considering both efficiency and accuracy. For one thing, in order to speed up, it applies interior warping to obtain deep context features. For another, different from previous warping methods, the non-key-frame CNN preserves several shallow *head* layers to add spatial features. Then, the two kinds of features are fused by lateral connections as FPN (Lin et al., 2017) and U-Net (Ronneberger et al., 2015). Meanwhile, it is worth noting that the spatial features are also provided to the correction modules as the input.

### 4.3 The Correction Stage

Inspired by this correction step in video codecs, we propose to add a correction step (right part of Fig. 3(b)) in our segmentation pipeline. The correction stage consists of two key modules. The Context Feature Rectification (CFR) module corrects the warped features, and the Residual-Guided Attention (RGA) module guides the learning of CFR.

#### 4.3.1 Context Feature Rectification

Although the non-key-frame CNN can add spatial details by employing low-level features via lateral connections, still, the errors in context feature would accumulate during successive feature warping. Thus, we claim the warped context features themselves need to be corrected. Comparing the pipeline of video codecs with warping-based segmentation methods (Fig. 3), we find the main problem of previous methods is the lack of a correction stage, which leads to inaccurate predictions and the error accumulation issue.

Inspired by the correction step in video codecs, we introduce the lightweight Context Feature Rectification (CFR) module to explicitly correct the warped context features. We design the CFR module considering the following aspects. First, the contextual information of the warped features is generally correct, except for the *edges of moving objects*. Second, the low-level features contain the spatial information, such as “edge” and “shape”. Thus, we claim the shape information in low-level features can help to correct the context feature, and we apply feature aggregation to perform this correction. CFR takes the warped context features  $\hat{\mathcal{F}}_t$  as well as the spatial features of the current frame  $f_t$  as the inputs and outputs the corrected context features  $\mathcal{F}_t$ , as shown in Fig. 5(a). Specifically, the CFR module adopts a single-layer network,  $\phi_r$ , which takes the concatenation  $[\hat{\mathcal{F}}_t, f_t]$  as the input and outputs the residual in feature space,  $Res\mathcal{F}_t$ . The mathematical form of

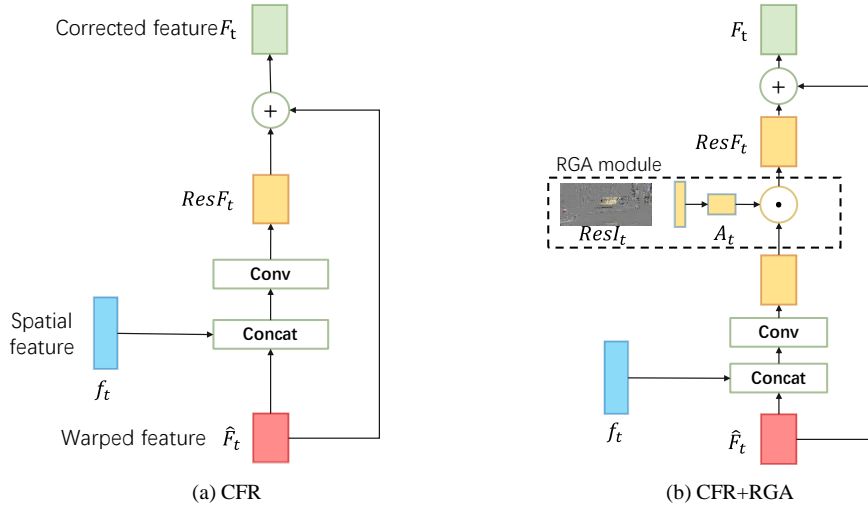


**Fig. 5** Details of (a) CFR and (b) CFR+RGA. “ $\odot$ ”: element-wise multiplication; “+”: element-wise addition.

CFR is defined as

$$\begin{aligned} \mathcal{F}_t &= \hat{\mathcal{F}}_t + \phi_r([\hat{\mathcal{F}}_t, f_t]) \\ &= \text{warp}(\mathcal{F}_{t-1}, Mv_t) + \text{Res}\mathcal{F}_t. \end{aligned} \quad (5)$$

During the training of CFR, in addition to the commonly used softmax cross entropy loss  $\mathcal{L}_{cls}$  for pixel-level classification, we propose to employ an L2 consistency loss  $\mathcal{L}_{consist}$  to minimize the distance between the corrected context features and the features extracted by the per-frame CNN.

#### 4.3.2 Residual-Guided Attention

To guide the learning of CFR and further improve its performance, we propose the Residual-Guided Attention (RGA) module.

In our TWNet, the motion vectors used for feature warping are the same as those used in image warping. Therefore, the *biases/errors should appear in the same spatial regions* in image space and feature space. Thus, the residual maps in image space  $\text{Res}I_t$  can be used as prior information to guide the learning of residuals in feature space  $\text{Res}\mathcal{F}_t$ . To realize this guidance, we adopt a lightweight spatial attention module named RGA to let the CFR module focus more on the regions with higher responses in  $\text{Res}I_t$ . Specifically, we first resize the residual map  $\text{Res}I_t$  to the shape of the warped context features. Then, we calculate the spatial attention map  $\mathcal{A}_t$  using a single-layer feed-forward CNN  $\phi_a$  as follows

$$\mathcal{A}_t = \phi_a(\text{Res}I_t). \quad (6)$$

Finally, we apply spatial attention by performing element-wise multiplication between  $\mathcal{A}_t$  and  $\text{Res}\mathcal{F}_t$ . Fig. 5(b) illustrates the detailed structure of RGA. After applying

this module, we formulate the whole process of TWNet for non-key frames, defined as

$$\mathcal{F}_t = \hat{\mathcal{F}}_t + \mathcal{A}_t \odot \text{Res}\mathcal{F}_t. \quad (7)$$

## 4.4 Implementation Details

### 4.4.1 Motion Extraction and Key Frame Selection

In our TWNet, we utilize *motion vectors* as motion maps. Both *motion vectors* and *residuals* are already contained in compressed videos. Thus, it takes no extra time to extract them. As for key frame scheduling, we simply regard all I-frames as key frames and P-frames as non-key frames, where I/P-frames are the concepts in video compression. An I-frame (Intra-coded picture) is stored as a complete image, while a P-frame (Predicted picture) is stored by the corresponding motion vectors and residual. Following previous works of (Shou et al., 2019; Wu et al., 2018), we choose MPEG-4 Part 2 (Simple Profile) (Sofokleous, 2005) as the compression standard, where each group of picture (GOP) contains an I-frame followed by 11 P-frames.

### 4.4.2 Layer Selection in the Non-Key-Frame CNN

It is worth noting that the layer of feature map used for warping can be arbitrarily chosen. In general, if we choose a deeper layer, there will be less corresponding *head* and *tail layers* (Fig. 6), since layers in the encoder-decoder architecture are paired by lateral connections. Thus, we will obtain a faster while less accurate model. Practically, we can adjust this hyperparameter to strike a balance between speed and accuracy.



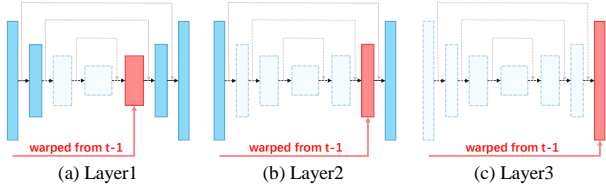


**Fig. 6** Choices of different layers for interior warping. The chosen layer is indicated with red color. The dotted arrows and boxes denote skipped operations.

#### 4.4.3 Training of TWNet

In general, the training of TWNet contains two main steps, i.e., the training of the per-frame CNN and the training of the non-key-frame CNN. The training of the per-frame CNN is similar to that of other image segmentation methods, where the softmax cross entropy loss  $\mathcal{L}_{cls}$  and the regularization loss  $\mathcal{L}_{reg}$  are used. Then, we fix all the parameters in the per-frame model (the key-frame CNN) and start to train the modules in the non-key-frame CNN. As mentioned in Sec. 4.3, we employ an additional L2 consistency loss  $\mathcal{L}_{consist}$  to minimize the distance between the corrected features and the context features extracted from the key-frame CNN. The object function of this training step is defined as

$$\mathcal{L} = \mathcal{L}_{cls} + \lambda_0 \mathcal{L}_{reg} + \lambda_1 \mathcal{L}_{consist}, \quad (8)$$

where  $\lambda_0$  and  $\lambda_1$  are weights to balance different kinds of losses.

During inference, we leave out the consistency loss since only one path (i.e., either the key-frame CNN or non-key-frame CNN) is used.

## 5 Experiments

In this section, we present the experimental results of TWNet on high-resolution videos. First, we introduce the experimental environment. Then, we perform ablation study to validate the effectiveness of the proposed non-key-frame CNN, CFR, and RGA. Finally, we compare TWNet with the state-of-the-art semantic video segmentation methods.

### 5.1 Experimental Setup

#### 5.1.1 Dataset

There are several commonly used datasets (e.g., Cityscapes (Cordts et al., 2016), CamVid (Brostow et al., 2009), COCO-Stuff (Caesar et al., 2018), and ADE20K (Zhou et al., 2017, 2019)) for semantic segmentation. We perform training and evaluation on the Cityscapes dataset

(Cordts et al., 2016) considering its high-resolution property and the requirements that the inputs should be video clips rather than images. Cityscapes contains 5000 high-resolution finely annotated images, which are divided into 2975, 500, and 1525 for training, validation and testing respectively. Each image is the 20<sup>th</sup> frame of a  $1024 \times 2048$  video clip. The dataset contains 19 classes for training and evaluation.

We perform the ablation study on the validation set of Cityscapes and compare the results of TWNet with the state-of-the-art methods. Also, we perform experiments on CamVid to demonstrate that our framework is generic to different datasets.

#### 5.1.2 Training

The training of TWNet is divided into two steps, i.e., the training of per-frame CNN and the training of the non-key-frame CNN. To train the per-frame model, we use the 2975 fine-annotated training images (i.e., the 20<sup>th</sup> frames in the video clips). We use MobileNet (Howard et al., 2017) pre-trained on ImageNet (Russakovsky et al., 2015) as the encoder of the key-frame CNN, and use three cascaded lateral connections (Lin et al., 2017) as the decoder. We apply the Adam optimizer (Kingma and Ba, 2014) to train for 90K iterations with the initial learning rate of  $1 \times 10^{-2}$  and batch size 8. We update the pre-trained parameters with 100 times smaller learning rate. Weight decay  $\lambda_0$  is set to  $1 \times 10^{-7}$ . Training data augmentations include mean extraction, random scaling between 0.5 to 2.0, random horizontal flipping, and random cropping to  $[800, 800]$  ( $[600, 600]$  for CamVid). We implement the model using TensorFlow 1.12 (Abadi et al., 2016) and perform training on a single GTX 1080 Ti GPU card.

After the training of per-frame CNN, the parameters in it are fixed, and we start to train the non-key-frame CNN. In each training step of non-key-frame CNN, we first send a batch of the 19<sup>th</sup> frames into the per-frame CNN to extract their context features. Then, we perform warping and correction for the corresponding 20<sup>th</sup> frames and calculate the loss according to Eq. (8). Note that if the consistency loss  $\mathcal{L}_{consist}$  is employed, the 20<sup>th</sup> frames should also be sent to the per-frame model to calculate the context features. In this training phase, random cropping is not adopted since the warping operation may exceed the cropped boundary. We set training size to  $[1024, 2048]$  ( $[720, 960]$  for CamVid) with batch size 4.

#### 5.1.3 Evaluation

In the inference phase, we conduct all the experiments on video clips with the resolution of  $1024 \times 2048$ . Dur-

**Table 1** Performance comparison of different layers used for interior warping. Interior warping: the layer of feature map used for interior warping; Fine-tuned: whether the second training step is performed to fine-tune the non-key-frame CNN. If not, the parameters of the head and tail layers keep the same as those in the per-frame CNN. If Layer 3 is chosen, there exists no trainable parameters and hence no fine-tuning.

| Warping Layer | Fine-tuned | mIoU | FPS   |
|---------------|------------|------|-------|
| Layer 1       | ✓          | 67.3 | 65.5  |
|               |            | 69.6 | 65.5  |
| Layer 2       | ✓          | 65.4 | 89.8  |
|               |            | 67.8 | 89.8  |
| Layer 3       | -          | 63.2 | 119.7 |

ing evaluation, the key frame is uniformly sampled from the 9<sup>th</sup> to the 20<sup>th</sup> frame in the video clip, and the prediction of the 20<sup>th</sup> frame is used for evaluation. No testing augmentation (e.g., multi-scale or multi-crop) is adopted. The accuracy is measured by mean Intersection-Over-Union (mIoU), and the speed is measured by frames per second (FPS). Our models run on a server with an Intel Core i9-7920X CPU and a single NVIDIA GeForce GTX 1080 Ti GPU card.

## 5.2 Ablation Study

We start building TWNet from the training of the per-frame model. We adopt the commonly used lightweight CNN, MobileNetV1, as the encoder. Our per-frame model achieves the accuracy of 73.6% mIoU at 35.5 FPS.

### 5.2.1 The Non-Key-Frame CNN

As described in Sec. 4.2, in the non-key-frame CNN, the layer of feature maps can be arbitrarily chosen to balance the accuracy and speed. We choose three layers in the decoder as the context features respectively. Results are summarized in Table 1.

According the experimental results, fine-tuning (the second training step) can significantly improve the performance. This demonstrates that low-level spatial features are more discriminative in the non-key-frame CNN, possibly due to the fact that the warped context features are less reliable in the non-key-frame CNN, thus the model depends more on low-level spatial features.

### 5.2.2 CFR Module and Consistency Loss

We propose the CFR module to correct the warped context features. As shown in Table 2, the CFR module is effective and efficient. Table 2 also demonstrates the effectiveness of consistency loss,  $\mathcal{L}_{consist}$ , and the weight

**Table 2** Validation of  $\mathcal{L}_{consist}$  during the training of CFR.  $\lambda_1$ : the weight of  $\mathcal{L}_{consist}$ .

| Warping Layer | $\lambda_1$ | mIoU        | FPS  |
|---------------|-------------|-------------|------|
| Layer 1       | 0           | 69.9        | 63.1 |
|               | 1           | 70.2        | 63.1 |
|               | 10          | <b>70.6</b> | 63.1 |
|               | 20          | 70.3        | 63.1 |
| Layer 2       | 0           | 67.6        | 86.3 |
|               | 1           | 68.1        | 86.3 |
|               | 10          | <b>68.6</b> | 86.3 |
|               | 20          | 68.3        | 86.3 |

**Table 3** Effect of each module of TWNet. FT: the fine-tuning of the non-key CNN (the second training step); CFR: Context Feature Rectification; RGA: Residual-Guided Attention. “✓” means the model utilizes the corresponding module. We also show the extra cost of adding our modules.

| Warping Layer | FT | CFR | RGA | mIoU        | FPS  | GFLOPs  |
|---------------|----|-----|-----|-------------|------|---------|
| Layer 1       |    |     |     | 67.3        | 65.5 | 113.28  |
|               | ✓  |     |     | 69.6        | 65.5 | +0      |
|               | ✓  | ✓   |     | 70.6        | 63.1 | +2.42   |
|               | ✓  | ✓   | ✓   | <b>71.6</b> | 61.8 | +0.0012 |
| Layer 2       |    |     |     | 65.4        | 89.8 | 73.00   |
|               | ✓  |     |     | 67.8        | 89.8 | +0      |
|               | ✓  | ✓   |     | 68.6        | 86.3 | +2.42   |
|               | ✓  | ✓   | ✓   | <b>69.5</b> | 84.9 | +0.0029 |

term,  $\lambda_1$ , a crucial hyper-parameter for the training of CFR. By default, we set  $\lambda_1$  to 10 in the following sections for better performance.

### 5.2.3 RGA Module

We introduce the RGA module to further exploit the correlation between residuals in image space and feature space. Results are demonstrated in Table 3. As expected, the RGA module further improves the performance of TWNet since it guides the CFR module to pay more attention to error-prone regions. The qualitative results of TWNet on Cityscapes are shown in Fig. 7.

### 5.2.4 Category-Level Improvement

The IoU improvements for different categories are shown in Table 4. The IoUs of **non-rigid objects** (human, object and vehicle) are improved greatly because of the following reasons. Since the motions of these moving objects are hard to predict, thus, the warped results are inaccurate. Our correction modules correct the wrong predictions and thus improve the accuracy.



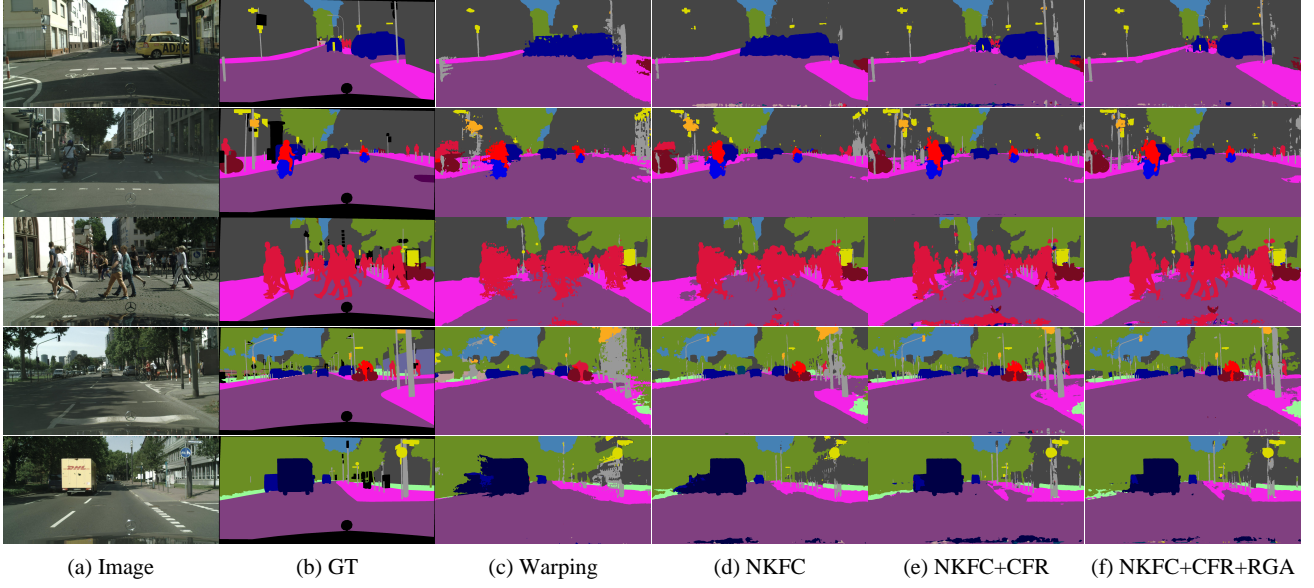
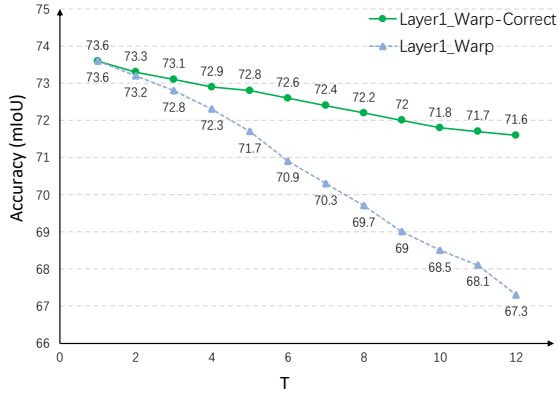


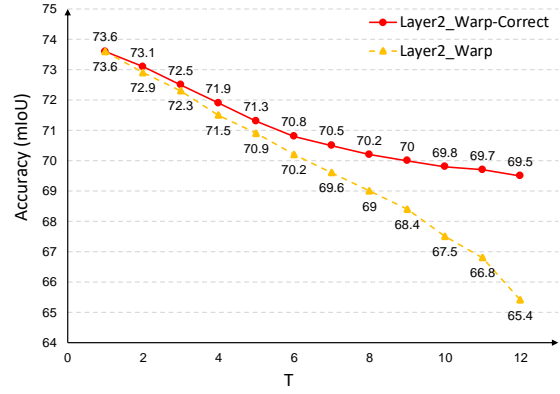
**Fig. 7** Qualitative results on the Cityscapes dataset. GT: ground truth; Warping: normal warping; NKFC: the non-key-frame CNN; CFR: context feature rectification; RGA: residual-guided attention.

**Table 4** IoU improvements of different categories. We choose Layer1 here.

| Method                       | object       | human        | vehicle     | nature      | construction | sky         | flat        |
|------------------------------|--------------|--------------|-------------|-------------|--------------|-------------|-------------|
| Warping                      | 43.8         | 56.7         | 82.2        | 86.6        | 87.1         | 91.6        | 96.6        |
| NKFC (The non-key-frame CNN) | 51.2 (+7.4)  | 65.5 (+8.8)  | 84.6 (+2.4) | 89.6 (+3.0) | 89.1 (+2.0)  | 94.0 (+2.4) | 97.3 (+0.7) |
| NKFC + CFR                   | 62.2 (+18.4) | 75.2 (+18.5) | 89.7 (+7.5) | 91.3 (+4.7) | 90.8 (+3.7)  | 94.2 (+2.6) | 97.9 (+1.3) |
| NKFC + CFR + RGA             | 62.2 (+18.4) | 76.1 (+19.4) | 90.1 (+7.9) | 91.1 (4.5)  | 91.0 (+3.9)  | 94.2 (+2.6) | 98.0 (+1.4) |



(a) Layer1



(a) Layer2

**Fig. 8** Performance degradation of Warp and Warp-Correct. (a): Layer 1 used for interior warping. (b): Layer 2 used for warping.  $T$ : frame interval between the key frame and the frame to be evaluated. The correction module effectively alleviates the long-term error accumulation problem.

### 5.2.5 Error Accumulation

We also conduct experiments to show that TWNNet is able to alleviate the error accumulation problem during consecutive warping. Suppose  $T$  denotes the frame-level interval between the initial key frame and the frame to be evaluated. We set  $T$  to different values and evaluate the performance of TWNNet and the non-key frame CNN

without correction modules. Results in Fig. 8 show that the correction modules significantly alleviate the accuracy degradation and improve the robustness of the models. Meanwhile, the employment of CFR and RGA takes little extra time.

**Table 5** Comparison of state-of-the-art semantic video segmentation models on Cityscapes. **Terms with “-pf”: mIoU/FPS for per-frame model**; “FPS norm” is calculated based on the performance of GPU. For previous works, we report the results in the **most comparable evaluation settings** to ours.

| Model                               | train set | eval set | resolution         | mIoU-pf | mIoU | FPS-pf | FPS  | FPS norm | GPU        |
|-------------------------------------|-----------|----------|--------------------|---------|------|--------|------|----------|------------|
| <i>Per-frame Models</i>             |           |          |                    |         |      |        |      |          |            |
| ICNet (Zhao et al., 2018)           | train     | val      | $1024 \times 2048$ | 67.7    | -    | 30.3   | -    | 49.7     | TITAN X(M) |
| ERFNet (Romera et al., 2017)        | train     | test     | $1024 \times 2048$ | 69.7    | -    | 11.2   | -    | 18.4     | TITAN X(M) |
| SwiftNetRN-18 (Orsic et al., 2019)  | train     | val      | $1024 \times 2048$ | 74.4    | -    | 34.0   | -    | 34.0     | 1080 Ti    |
| CAS (Zhang et al., 2019b)           | train     | val      | $1024 \times 2048$ | 74.0    | -    | 34.2   | -    | 48.9     | 1070       |
| <i>Video-based Models</i>           |           |          |                    |         |      |        |      |          |            |
| DFF (Zhu et al., 2017)              | train     | val      | $512 \times 1024$  | 71.1    | 69.2 | 1.52   | 5.6  | 12.8     | Tesla K40  |
| DVSNet1 (Xu et al., 2018)           | train     | val      | $1024 \times 2048$ | 73.5    | 63.2 | 5.6    | 30.4 | 30.4     | 1080 Ti    |
| DVSNet2 (Xu et al., 2018)           | train     | val      | $1024 \times 2048$ | 73.5    | 70.4 | 5.6    | 19.8 | 19.8     | 1080 Ti    |
| Prop-mv (Jain and Gonzalez, 2018)   | train     | val      | $1024 \times 2048$ | 75.2    | 61.7 | 1.3    | 7.6  | 9.6      | Tesla K80  |
| Interp-mv (Jain and Gonzalez, 2018) | train     | val      | $1024 \times 2048$ | 75.2    | 66.6 | 1.3    | 7.2  | 9.1      | Tesla K80  |
| Low-Latency (Li et al., 2018)       | train     | val      | $1024 \times 2048$ | 80.2    | 75.9 | 2.8    | 8.4  | -        | -          |
| <i>Ours</i>                         |           |          |                    |         |      |        |      |          |            |
| TWNet-Layer1                        | train     | val      | $1024 \times 2048$ | 73.6    | 71.6 | 35.5   | 61.8 | 61.8     | 1080 Ti    |
| TWNet-Layer1                        | train     | test     | $1024 \times 2048$ | 73.1    | 71.2 | 35.5   | 61.8 | 61.8     |            |
| TWNet-Layer2                        | train     | val      | $1024 \times 2048$ | 73.6    | 69.5 | 35.5   | 84.9 | 84.9     |            |
| TWNet-Layer2                        | train     | test     | $1024 \times 2048$ | 73.1    | 69.0 | 35.5   | 84.9 | 84.9     |            |

### 5.2.6 Choices of Backbones

We study the genericity of our TWNet to different backbones. We show the results based on other lightweight backbones, i.e., MobileNetV2 and ResNet-18.

As described in Section 4.4.2, we can choose different layers of the decoder for interior feature warping to create different versions of TWNet (as illustrated in Fig. 6). Table 6 shows the required *head* layers for each version.

**Table 6** The required *head* layers for different versions of TWNet. *head<sub>n</sub>*: the  $n^{th}$  *head* layer of the encoder.

| Model name   | head1 | head2 | head3 |
|--------------|-------|-------|-------|
| Per-frame    | ✓     | ✓     | ✓     |
| TWNet-Layer1 | ✓     | ✓     |       |
| TWNet-Layer2 | ✓     |       |       |
| TWNet-Layer3 |       |       |       |

The head layers for different backbones are defined in Table 7. We use the notations from the TensorFlow Slim package.

**Table 7** *Head* layers for different backbones. We quote the notations from the TensorFlow Slim package.

| Backbone    | head1           | head2           | head3            |
|-------------|-----------------|-----------------|------------------|
| MobileNetV1 | <i>conv2d_3</i> | <i>conv2d_5</i> | <i>conv2d_11</i> |
| MobileNetV2 | <i>layer_4</i>  | <i>layer_7</i>  | <i>layer_14</i>  |
| ResNet-18   | <i>conv2_2</i>  | <i>conv3_2</i>  | <i>conv4_2</i>   |

**Table 8** Performance of TWNet based on different backbone networks. IW: the layer we use to do interior warping. “None” means no interior warping.

| Backbone    | IW     | mIoU | FPS   | Speed-up ( $\times$ ) |
|-------------|--------|------|-------|-----------------------|
| MobileNetV1 | None   | 73.6 | 35.5  | -                     |
|             | Layer1 | 71.6 | 61.8  | 1.74                  |
|             | Layer2 | 69.5 | 84.9  | 2.39                  |
|             | Layer3 | 63.2 | 119.7 | 3.37                  |
| MobileNetV2 | None   | 73.2 | 32.3  | -                     |
|             | Layer1 | 71.3 | 59.6  | 1.85                  |
|             | Layer2 | 69.4 | 82.5  | 2.55                  |
|             | Layer3 | 62.4 | 115.8 | 3.59                  |
| ResNet-18   | None   | 71.6 | 36.9  | -                     |
|             | Layer1 | 69.4 | 63.6  | 1.72                  |
|             | Layer2 | 67.7 | 86.8  | 2.35                  |
|             | Layer3 | 61.9 | 120.4 | 3.26                  |

Table 8 shows the experimental results of TWNet based on different backbones. In summary, TWNet is generic to backbone networks, and hence can be adapted to various per-frame models for different requirements of speed and accuracy.

### 5.2.7 Choices of Flow Models

We could use optical flow methods, e.g., FlowNet2 (Ilg et al., 2017) and PWC-Net (Sun et al., 2018), as the flow model of our framework. However, the running speeds of these methods are even slower than our key-frame segmentation network (even slower than 20 fps), which means the warping operation will not speed up the inference phase. Also, when we use these optical-flow methods as warping, the segmentation accuracy is similar to our motion-vector version. Thus, we decide

**Table 9** Effect of different flow models.

| Flow model     | mIoU | FPS  |
|----------------|------|------|
| Motion vectors | 67.3 | 65.5 |
| FlowNet2       | 67.5 | 13.2 |
| FlowNet2-s     | 66.3 | 26.6 |
| FlowNet2-c     | 66.6 | 22.7 |
| PWC-Net        | 67.0 | 29.4 |

to use motion vectors. Table 9 shows the accuracy using different types of flows for warping.

### 5.3 Comparison with Other Methods

We compare the proposed TWNNet with other state-of-the-art semantic video segmentation models, as shown in Table 5. Note that the speed (FPS) values measured in different models are just listed for reference, since the experimental environments may vary a lot. All of our models run on the platform with CUDA 9.2, cuDNN 7.3 and TensorFlow 1.12, and we use the *timeline* tool in TensorFlow to measure the speed. Following the recent work of (Orsic et al., 2019), we include the “FPS norm” value based on the GPU types of previous methods<sup>1</sup>. Results demonstrate that our TWNNet achieves the highest inference speed with comparable accuracy on inputs at a resolution of  $1024 \times 2048$ . Also, the accuracy of TWNNet decreases more slightly than other video-based methods. It is worth noting that we adopt the key-frame CNN to simplify our presentation. If a more delicate per-frame model were used, the performance of TWNNet would be further improved.

### 5.4 Results on the CamVid Dataset

We also conduct experiments on the CamVid dataset, which contains 367, 100, 233 720  $\times$  960 video clips for training, validation and testing. We apply the same configurations as those of Cityscapes except for the crop size. As shown in Table 10 and Table 11, TWNNet achieves consistent results on CamVid.

## 6 Conclusion

We present a novel framework TWNNet for real-time high-resolution semantic video segmentation. Specifically, we use warping and employ the non-key-frame CNN architecture for acceleration. In order to alleviate the errors caused by feature warping, we propose two

**Table 10** Effect of each module of TWNNet on the CamVid test set.

| Warping Layer | FT | CFR | RGA | mIoU        | FPS   |
|---------------|----|-----|-----|-------------|-------|
| Layer 1       |    |     |     | 68.8        | 183.1 |
|               | ✓  |     |     | 69.9        | 183.1 |
|               | ✓  | ✓   |     | 71.0        | 179.8 |
|               | ✓  | ✓   | ✓   | <b>71.5</b> | 175.2 |
| Layer 2       |    |     |     | 66.7        | 252.6 |
|               | ✓  |     |     | 68.1        | 252.6 |
|               | ✓  | ✓   |     | 69.3        | 245.8 |
|               | ✓  | ✓   | ✓   | <b>70.0</b> | 240.7 |

**Table 11** Comparison with other methods on the CamVid test set.

| Model                               | mIoU-pf | mIoU | FPS-pf | FPS   |
|-------------------------------------|---------|------|--------|-------|
| DFANet A (Li et al., 2019a)         | 64.7    | -    | 120    | -     |
| ICNet (Zhao et al., 2018)           | 67.1    | -    | 27.8   | -     |
| BiSeNet (Yu et al., 2018)           | 68.7    | -    | -      | -     |
| Prov-mv (Jain and Gonzalez, 2018)   | 68.6    | 63.4 | 3.8    | 21.4  |
| Interp-mv (Jain and Gonzalez, 2018) | 68.6    | 67.3 | 3.8    | 19.1  |
| TWNNet-Layer1                       | 73.5    | 71.5 | 103.5  | 175.2 |
| TWNNet-Layer2                       | 73.5    | 70.0 | 103.5  | 240.7 |

efficient modules, namely CFR and RGA, to correct the warped features by learning the feature-space residual. Experimental results demonstrate that our method is much more robust than warping-based approaches while keeps the high speed.

## References

- Abadi M, Barham P, Chen J, Chen Z, Davis A, Dean J, Devin M, Ghemawat S, Irving G, Isard M, et al. (2016) Tensorflow: A system for large-scale machine learning. In: 12th USENIX Symposium on Operating Systems Design and Implementation 16), pp 265–283
- Badrinarayanan V, Kendall A, Cipolla R (2017) Segnet: A deep convolutional encoder-decoder architecture for image segmentation. *IEEE transactions on pattern analysis and machine intelligence* 39(12):2481–2495
- Brostow GJ, Fauqueur J, Cipolla R (2009) Semantic object classes in video: A high-definition ground truth database. *Pattern Recognition Letters* 30(2):88–97
- Caesar H, Uijlings J, Ferrari V (2018) COCO-stuff: Thing and stuff classes in context. In: *Proceedings of the IEEE Conference on Computer Vision and Pattern Recognition*, pp 1209–1218
- Chen LC, Zhu Y, Papandreou G, Schroff F, Adam H (2018) Encoder-decoder with atrous separable convolution for semantic image segmentation. In: *Proceedings of the European conference on computer vision*, pp 801–818

<sup>1</sup> GPU Benchmark: [www.techpowerup.com/gpu-specs](http://www.techpowerup.com/gpu-specs)

- Cordts M, Omran M, Ramos S, Rehfeld T, Enzweiler M, Benenson R, Franke U, Roth S, Schiele B (2016) The cityscapes dataset for semantic urban scene understanding. In: Proceedings of the IEEE conference on computer vision and pattern recognition, pp 3213–3223
- Fu J, Liu J, Tian H, Li Y, Bao Y, Fang Z, Lu H (2019) Dual attention network for scene segmentation. In: Proceedings of the IEEE Conference on Computer Vision and Pattern Recognition, pp 3146–3154
- Gadde R, Jampani V, Gehler PV (2017) Semantic video cnns through representation warping. In: Proceedings of the IEEE International Conference on Computer Vision, pp 4453–4462
- He J, Deng Z, Qiao Y (2019) Dynamic multi-scale filters for semantic segmentation. In: Proceedings of the IEEE International Conference on Computer Vision, pp 3562–3572
- Howard AG, Zhu M, Chen B, Kalenichenko D, Wang W, Weyand T, Andreetto M, Adam H (2017) Mobilenets: Efficient convolutional neural networks for mobile vision applications. arXiv preprint arXiv:1704.04861
- Hu P, Caba F, Wang O, Lin Z, Sclaroff S, Perazzi F (2020) Temporally distributed networks for fast video semantic segmentation. In: Proceedings of the IEEE/CVF Conference on Computer Vision and Pattern Recognition, pp 8818–8827
- Huang Z, Wang X, Huang L, Huang C, Wei Y, Liu W (2019) Ccnet: Criss-cross attention for semantic segmentation. In: Proceedings of the IEEE International Conference on Computer Vision, pp 603–612
- Ilg E, Mayer N, Saikia T, Keuper M, Dosovitskiy A, Brox T (2017) FlowNet 2.0: Evolution of optical flow estimation with deep networks. In: Proceedings of the IEEE Conference on Computer Vision and Pattern Recognition, pp 2462–2470
- Jain S, Gonzalez JE (2018) Fast semantic segmentation on video using block motion-based feature interpolation. In: European Conference on Computer Vision, Springer, pp 3–6
- Kingma DP, Ba J (2014) Adam: A method for stochastic optimization. arXiv preprint arXiv:1412.6980
- Le Gall D (1991) Mpeg: A video compression standard for multimedia applications. Communications of the ACM 34(4):46–59
- Li H, Xiong P, Fan H, Sun J (2019a) DFANet: Deep feature aggregation for real-time semantic segmentation. In: Proceedings of the IEEE Conference on Computer Vision and Pattern Recognition, pp 9522–9531
- Li X, Zhou Y, Pan Z, Feng J (2019b) Partial order pruning: for best speed/accuracy trade-off in neural architecture search. In: Proceedings of the IEEE Conference on Computer Vision and Pattern Recognition, pp 9145–9153
- Li Y, Shi J, Lin D (2018) Low-latency video semantic segmentation. In: Proceedings of the IEEE Conference on Computer Vision and Pattern Recognition, pp 5997–6005
- Lin TY, Dollár P, Girshick R, He K, Hariharan B, Belongie S (2017) Feature pyramid networks for object detection. In: Proceedings of the IEEE conference on computer vision and pattern recognition, pp 2117–2125
- Long J, Shelhamer E, Darrell T (2015) Fully convolutional networks for semantic segmentation. In: Proceedings of the IEEE conference on computer vision and pattern recognition, pp 3431–3440
- Orsic M, Kreso I, Bevandic P, Segvic S (2019) In defense of pre-trained imagenet architectures for real-time semantic segmentation of road-driving images. In: Proceedings of the IEEE Conference on Computer Vision and Pattern Recognition, pp 12607–12616
- Romera E, Alvarez JM, Bergasa LM, Arroyo R (2017) ERFNet: Efficient residual factorized convnet for real-time semantic segmentation. IEEE Transactions on Intelligent Transportation Systems 19(1):263–272
- Ronneberger O, Fischer P, Brox T (2015) U-net: Convolutional networks for biomedical image segmentation. In: International Conference on Medical image computing and computer-assisted intervention, Springer, pp 234–241
- Russakovsky O, Deng J, Su H, Krause J, Satheesh S, Ma S, Huang Z, Karpathy A, Khosla A, Bernstein M, et al. (2015) ImageNet large scale visual recognition challenge. International journal of computer vision 115(3):211–252
- Sandler M, Howard A, Zhu M, Zhmoginov A, Chen LC (2018) Mobilenetv2: Inverted residuals and linear bottlenecks. In: Proceedings of the IEEE Conference on Computer Vision and Pattern Recognition, pp 4510–4520
- Shou Z, Lin X, Kalantidis Y, Sevilla-Lara L, Rohrbach M, Chang SF, Yan Z (2019) DMC-Net: Generating discriminative motion cues for fast compressed video action recognition. In: Proceedings of the IEEE Conference on Computer Vision and Pattern Recognition, pp 1268–1277
- Sofokleous A (2005) H. 264 and MPEG-4 video compression: Video coding for next-generation multimedia
- Sun D, Yang X, Liu MY, Kautz J (2018) Pwc-net: Cnns for optical flow using pyramid, warping, and cost volume. In: Proceedings of the IEEE Conference on Computer Vision and Pattern Recognition, pp 8934–

8943

- Wu CY, Zaheer M, Hu H, Manmatha R, Smola AJ, Krähenbühl P (2018) Compressed video action recognition. In: Proceedings of the IEEE Conference on Computer Vision and Pattern Recognition, pp 6026–6035
- Xu YS, Fu TJ, Yang HK, Lee CY (2018) Dynamic video segmentation network. In: Proceedings of the IEEE Conference on Computer Vision and Pattern Recognition, pp 6556–6565
- Yu C, Wang J, Peng C, Gao C, Yu G, Sang N (2018) BiSeNet: Bilateral segmentation network for real-time semantic segmentation. In: Proceedings of the European Conference on Computer Vision, pp 325–341
- Zach C, Pock T, Bischof H (2007) A duality based approach for realtime TV-L 1 optical flow. In: Joint pattern recognition symposium, Springer, pp 214–223
- Zhang H, Zhang H, Wang C, Xie J (2019a) Co-occurrent features in semantic segmentation. In: Proceedings of the IEEE Conference on Computer Vision and Pattern Recognition, pp 548–557
- Zhang Y, Qiu Z, Liu J, Yao T, Liu D, Mei T (2019b) Customizable architecture search for semantic segmentation. In: Proceedings of the IEEE Conference on Computer Vision and Pattern Recognition, pp 11641–11650
- Zhao H, Shi J, Qi X, Wang X, Jia J (2017) Pyramid scene parsing network. In: Proceedings of the IEEE conference on computer vision and pattern recognition, pp 2881–2890
- Zhao H, Qi X, Shen X, Shi J, Jia J (2018) ICNet for real-time semantic segmentation on high-resolution images. In: Proceedings of the European Conference on Computer Vision, pp 405–420
- Zhou B, Zhao H, Puig X, Fidler S, Barriuso A, Torralba A (2017) Scene parsing through ade20k dataset. In: Proceedings of the IEEE conference on computer vision and pattern recognition, pp 633–641
- Zhou B, Zhao H, Puig X, Xiao T, Fidler S, Barriuso A, Torralba A (2019) Semantic understanding of scenes through the ade20k dataset. *International Journal of Computer Vision* 127(3):302–321
- Zhu X, Xiong Y, Dai J, Yuan L, Wei Y (2017) Deep feature flow for video recognition. In: Proceedings of the IEEE Conference on Computer Vision and Pattern Recognition, pp 2349–2358
- Zhu Z, Xu M, Bai S, Huang T, Bai X (2019) Asymmetric non-local neural networks for semantic segmentation. In: Proceedings of the IEEE International Conference on Computer Vision, pp 593–602